Measurement and Modeling of Ultrawideband TOA-Based Ranging in Indoor Multipath Environments

Nayef A. Alsindi, *Student Member, IEEE*, Bardia Alavi, *Member, IEEE*, and Kaveh Pahlavan, *Fellow, IEEE*

***Abstract*—In this paper, we present the results of the measurement and modeling of ultrawideband (UWB) time of arrival (TOA)-based ranging in different indoor multipath environments. We provide a detailed characterization of the spatial behavior of ranging, where we focus on the statistics of the ranging error in the presence and absence of the direct path (DP) and evaluate the path loss behavior in the former case, which is important for indoor geolocation coverage characterization. The frequency-domain measurements were conducted, with a nominal frequency of 4.5 GHz with two different bandwidths, i.e., 500 MHz and 3 GHz. The parameters of the ranging error probability distributions and path loss models are provided for different environments (e.g., an old office, a modern office, a house, and a manufacturing floor) and different ranging scenarios [e.g., indoor to indoor (ITI), outdoor to indoor (OTI), and roof to indoor (RTI)].**

***Index Terms*—Indoor geolocation, nonline-of-sight (NLOS) ranging, ranging coverage, time of arrival (TOA)-based ranging, ultrawideband (UWB) localization.**

I. Introduction

RECENTLY, ultrawideband (UWB) technology has been one of the major developments in the wireless industry, with potential for high-data-rate communication and precise time of arrival (TOA)-based ranging [1]–[3]. Large bandwidths offer high resolution and signaling, which allows for centimeter accuracies and low-power and low-cost implementation [4]. Numerous potential applications have been identified for indoor localization in general and for UWB localization in particular [4]–[6]. Depending on the nature of the application, different ranging scenarios will be necessary for both traditional and wireless sensor networks. This means that scenarios will not be limited to indoor-to-indoor (ITI) ranging. Indeed, for a variety of applications (e.g., firefighters and soldiers in hostile buildings), rapid deployment of beacon infrastructure surrounding and located on top of buildings will be necessary. In these situations, outdoor-to-indoor (OTI) and roof-to-indoor (RTI) will impose different challenges to UWB ranging (see Fig. 1).

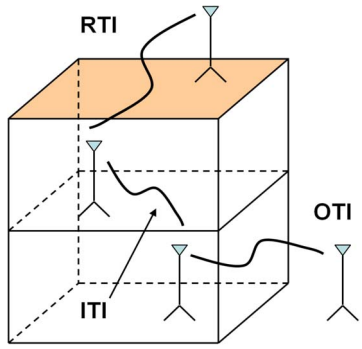

Fig. 1. Indoor ranging scenarios.

The performance of TOA-based UWB ranging systems depends on the availability of the direct path (DP) signal [7], [8]. In indoor environments, the DP can be detected in both line of sight (LOS) and non-LOS (NLOS). Similar to wireless communications terminology, NLOS refers to the absence of a physical LOS between the transmitter and receiver and *not* the absence of the DP. This means that, in these situations, the DP can be detected, albeit attenuated. In short-distance LOS, the DP is always detectable, and accurate UWB TOA estimates in the range of centimeters are feasible due to the high time-domain resolution [9], [10]. The challenge is UWB ranging in indoor NLOS conditions, which can be characterized as dense multipath environments [7], [8]. In these conditions, depending on the presence or absence of the DP, the ranging errors can significantly vary. Specifically, in the presence of the DP, the dominant sources of error are multipath and propagation delay. Multipath error corrupts the TOA estimates due to the multipath components (MPC), which are delayed and attenuated replicas of the original signal, arriving and combining at the receiver shifting the estimate. Propagation delay caused by the signal traveling through obstacles can further add a positive bias to the TOA estimates. Although UWB can mitigate multipath with the availability of excess bandwidth [10], [11], its ability to perform in the absence of the DP needs to be further investigated. In the absence of the DP [also referred to as undetected DP (UDP)] in [8] and [12], type-1 and -2 NLOS in [13], and late errors in [14], range estimates are corrupted by larger positive biases, which have a significant probability of occurrence due to cabinets, elevator shafts, or doors that are usually cluttering the

Manuscript received June 8, 2007; revised October 22, 2007, January 30, 2008, and March 29, 2008. First published May 23, 2008; current version published March 17, 2009. This work was supported in part by the Defense Advanced Research Projects Agency/Department of Defense under Small Business Innovative Research Grant BAA 03-029. The review of this paper was coordinated by Dr. X. Wang.

N. A. Alsindi and K. Pahlavan are with the Center for Wireless Information Network Studies, Worcester Polytechnic Institute, Worcester, MA 01609 USA (e-mail: nayefalsindi@gmail.com; kaveh@wpi.edu).

B. Alavi is with the Wireless Networking Business Unit, Cisco Systems Inc., Richfield, OH 44286 USA (e-mail: balavi@cisco.com).

Color versions of one or more of the figures in this paper are available online at http://ieeexplore.ieee.org.

Digital Object Identifier 10.1109/TVT.2008.926071

indoor environment. Furthermore, mitigation of this problem by increasing the system bandwidth alone has its limitations [12].

Characterization of the UWB channels for ranging applications is different from communications [5]. For the latter, the focus is on data rate and communication coverage through the characterization of the delay spread and the path loss of the total signal energy. The former, however, requires special attention on the ranging accuracy, i.e., the statistics of the ranging error and ranging coverage. Characterizing the probability of DP blockage and the statistics of the error in the presence and absence of the DP provides an understanding of the challenges and limitations imposed by the multipath environment. For the ranging coverage, characterizing the path loss-distance dependence of the DP in a given scenario and environment can provide practical indications of the maximum possible ranging distance [15].

UWB indoor propagation experiments have extensively been carried out [16]–[19], but these efforts mainly focus on the communication aspects of UWB. Several indoor propagation experiments with a focus on indoor ranging, be it UWB or otherwise, have been reported in [6]–[8], [10], [11], [13], and [20]–[25], which are usually limited to a floor or several rooms but do not address modeling the spatial statistics of NLOS ranging nor ranging coverage. The only available ranging error models were provided in [13] and [21] but are based on limited measurement data sets, and only the latter focuses on the characterization of errors according to the availability of the DP. As a result, a comprehensive measurement and modeling of the UWB TOA-based ranging in different indoor environments and scenarios is not available in the literature. These models are needed to provide a realistic platform for algorithm performance analysis. More importantly, they are necessary for determining localization performance bounds in NLOS cluttered environments [26], [27], which can provide insight into the fundamental limitations facing indoor UWB localization in both traditional wireless and sensor networks.

In this paper, we provide extensive measurement and modeling of the large-scale characteristics of UWB ranging in different scenarios and environments. Specifically, we provide measurements and models that characterize the spatial ranging error and coverage for ITI, OTI, and RTI scenarios in four different indoor environments: 1) a house; 2) an old office; 3) a modern office; and 4) a manufacturing floor.

The organization of this paper is given as follows: In Section II, we describe the challenges facing UWB TOA-based ranging in indoor environments. In Section III, we describe the measurement system, procedure, and postprocessing of measurement data. In Section IV, we provide ranging coverage analysis through empirical path loss models. In Section V, we provide spatial modeling of the ranging error. In Section VI, we validate our models through simulations. Finally, we conclude this paper in Section VII.

II. UWB TOA-Based Ranging

A. Background

One of the major factors determining the quality of TOA-based ranging in indoor geolocation is the ability to detect the DP between a reference point (RP) and a mobile terminal (MT) in the presence of dense multipath. For the indoor multipath channel, the impulse response is usually modeled as

$$h(\tau) = \sum_{k=1}^{L_p} \alpha_k e^{j\phi_k} \delta(\tau - \tau_k) \tag{1}$$

where L_p is the number of MPCs, and α_k, ϕ_k, and τ_k are the amplitude, phase, and propagation delay of the kth path, respectively [28]. When the DP is detected, $\alpha_1 = \alpha_{\mathrm{DP}}$, and $\tau_1 = \tau_{\mathrm{DP}}$, where α_{DP} and τ_{DP} denote the DP amplitude and propagation delay, respectively. The distance between the MT and the RP is $d_{\mathrm{DP}} = v \times \tau_{\mathrm{DP}}$, where v is the speed of signal propagation. In the absence of the DP, ranging can be achieved using the amplitude and propagation delay of the first non-DP (NDP) component given by α_{NDP} and τ_{NDP}, respectively, resulting in a longer distance given by $d_{\mathrm{NDP}} = v \times \tau_{\mathrm{NDP}}$, where $d_{\mathrm{NDP}} > d_{\mathrm{DP}}$. For the receiver to identify the DP, the ratio of the strongest MPC to the DP given by

$$\rho_1 = \left(\frac{\max\left(|\alpha_i|_{i=1}^{L_p} \right)}{|\alpha_{\mathrm{DP}}|} \right) \tag{2}$$

must be less than receiver dynamic range ρ, and the power of the DP must be greater than receiver sensitivity φ [29]. These constraints are given by

$$\rho_1 \leq \rho \tag{3a}$$

$$P_{\mathrm{DP}} > \varphi \tag{3b}$$

where $P_{\mathrm{DP}} = 20 \log_{10}(|\alpha_{\mathrm{DP}}|)$.

B. Ranging Coverage

Existing UWB indoor radio wave propagation measurements have mainly focused on determining the radio coverage in different environments. The reported results and models, however, are not adequate for predicting the coverage of TOA-based UWB indoor geolocation systems, because the performance in multipath-rich indoor environments depends on the signal-to-noise ratio (SNR) of the DP between the transmitter and the receiver. Unlike communication coverage, which is related to the received power of all the MPCs in a given distance, ranging coverage is related to the received power of the DP component. For a given system dynamic range ρ, we define ranging coverage R_c as the distance in which the maximum tolerable average path loss of the DP is within ρ [15]. This is represented by

$$\max\{\overline{PL_{\mathrm{DP}}}\} = 10\gamma \log_{10}(R_c) \leq \rho \tag{4}$$

where $\overline{PL_{\mathrm{DP}}}$ is the average path loss of the DP, and γ is the path loss exponent. The path loss behavior of the DP is distance dependent, but because of the attenuation and energy removed by scattering, its intensity more rapidly decreases with distance compared to the total signal energy [30]. This means that, for a typical indoor multipath scattering environment, communication coverage is greater than ranging coverage, i.e., $C_c > R_c$. Operating out of the ranging coverage causes large TOA estimation errors and performance degradation.

C. Ranging Error

Ranging and localization are constrained by the statistics of the ranging error, which is defined as the difference between the estimated and the actual distance or

$$\varepsilon = \hat{d} - d_{\mathrm{DP}}. \tag{5}$$

In an indoor environment, the MT experiences varying ranging-error behaviors, depending on the relative location of the MT to that of the RP. More specifically, it depends on the availability of the DP and, in the case of its absence, on the characteristics of the blockage. In this paper, we categorize the error based on the following ranging states. In the presence of the DP, both (3a) and (3b) are met, and the distance estimate is very accurate, yielding

$$\hat{d}_{\mathrm{DP}} = d_{\mathrm{DP}} + \varepsilon_{\mathrm{DP}} + n \tag{6a}$$

$$\varepsilon_{\mathrm{DP}} = \begin{cases} b_m(\omega), & \text{LOS} \\ b_m(\omega) + b_{\mathrm{pd}}, & \text{NLOS} \end{cases} \tag{6b}$$

where $b_m(\omega)$ is the bias induced by the multipath that dominates when the DP is present and is a function of the system's bandwidth ω [10], [11], b_{pd} is the propagation delay imposed by the NLOS condition, and n is zero-mean measurement noise. Similar to wireless communications terminology, we will use the NLOS term to denote the absence of a physical LOS between the transmitter and receiver and *not* the absence of the DP. This means that, in these situations, the DP can be detected, albeit attenuated.

When the MT is within ranging coverage but experiences sudden blockage of the DP, which is also known as UDP [8], (3a) is not met, and the DP is shadowed by some obstacle burying its power under the dynamic range of the receiver. In this situation, the ranging estimate experiences a larger bias error compared to (6). Emphasizing that ranging is achieved through the NDP component. The estimate is then given by

$$\hat{d}_{\mathrm{NDP}} = d_{\mathrm{DP}} + \varepsilon_{\mathrm{NDP}} + n \tag{7a}$$

$$\varepsilon_{\mathrm{NDP}} = b_m(\omega) + b_{\mathrm{pd}} + b_B(\omega) \tag{7b}$$

where $b_B(\omega)$ is an additive positive bias representing the nature of the blockage, and it dominates the error compared to measurement noise. Its dependence on bandwidth is through its impact on the energy per MPC. Higher bandwidth results in lower energy per MPC, which increases the probability of DP blockage. Finally, when the user operates outside of the ranging coverage, neither (3a) nor (3b) are met, and large errors occur with high probability.

Formally, these ranging states can be defined as follows:

$$\zeta_1 = \{\hat{d} = \hat{d}_{\mathrm{DP}} | d \le R_c\} \tag{8a}$$

$$\zeta_2 = \{\hat{d} = \hat{d}_{\mathrm{NDP}} | d \le R_c\} \tag{8b}$$

$$\zeta_3 = \{\hat{d} = \hat{d}_{\mathrm{NDP}} | d > R_c\} \tag{8c}$$

$$\zeta_4 = \{\hat{d} = \hat{d}_{\mathrm{DP}} | d > R_c\}. \tag{8d}$$

In this paper, we will focus on modeling the error statistics within the ranging coverage. The performance in ζ_3 is dominated by large measurement noise variations, which means that the significance of (6b) and (7b) diminishes [27]. We further assume that $p(\zeta_4) \approx 0$ since, from our definition in (4), the DP cannot be detected after the ranging coverage.

III. UWB Indoor Geolocation-Specific Measurement Campaign

A. Background

Frequency-domain measurement techniques have previously been employed to characterize the channel impulse response [17], [19], [28], [31]. The measurements provided the characterization of communication parameters, such as the RMS delay spread and power–distance relationship. In this paper, we follow the same techniques but measure the large-scale spatial characteristics of the DP, mainly $\hat{\alpha}_{\mathrm{DP}}$ and $\hat{\tau}_{\mathrm{DP}}$, which can be used to examine the ranging coverage (path loss characterization) and accuracy, respectively. In the absence of the DP, we measure the first detected path $\hat{\tau}_{\mathrm{NDP}}$ and analyze the probability of blockage and the error statistics under this condition.

B. Measurement System

The measurement system, which is similar to those in [17], [19], and [31], employs an Agilent E8363B vector network analyzer (VNA) that is used to sweep the frequency spectrum of 3–8 GHz with a sampling interval of 312.5kHz (16 001 sampling points). The VNA measures the S21 S-parameter, which is the transfer function of the channel. The transmitter and the receiver are a pair of disc-cone UWB antennas, which are connected to the VNA by low-loss high-quality doubly shielded cables. On the receiver side, a low-noise amplifier (LNA) is connected between the antenna and the VNA. On the transmitter side, a 30-dB power amplifier with a frequency range of 3–8 GHz further improves the dynamic range. The transmitter and receiver heights were fixed to 1.5 m. The overall measurement system has a dynamic range of 120 dB. The undesirable effects of the cables, LNA, and antennas are removed through system calibration.

C. Measurement Locations and Procedure

A comprehensive UWB propagation experiment was performed in four buildings: 1) a house located on 17 Schussler Road; 2) Fuller Laboratory–a modern office building; 3) a manufacturing floor in Norton Company; and 4) Atwater Kent (AK)–an old office building; all are located in Worcester, MA. The house on 17 Schussler Road is fairly big, with wooden exterior walls and Sheetrock interior walls. The rooms have dimensions on the order of a few meters and contain furniture, such as couches, tables, and chairs. Fuller Laboratories is a modern building characterized by external brick walls with some aluminum siding on two sides, and metallic window frames and doors.

The dimension of the building is on the order of a few tens of meters and contains several computer labs, department offices, and lecture halls. Norton Company is a manufacturer of welding equipment and abrasives for grinding machines with

TABLE I
SUMMARY OF THE MEASUREMENT DATABASE

Environment	Scenario	TX or RX Location	Description of the scenarios	Max. meas. range (m)	Num. of meas.
Office (Fuller Laboratories)	OTI	Entrance I & II	Multi-floor – close to the door	45	336
		Arbitrary	Multi-floor – away from door		150
	ITI	LOS	Open area around entrance	24	120
		NLOS	Inter-floor – open area	23	72
			Inter-floor – close area		54
Residential (17 Schussler Rd.)	OTI	Entrance I	Multi-floor – front	15	186
		Entrance II	Multi-floor – side		186
	ITI	NLOS	Same-floor	10	108
			Inter-floor		66
Factory (Norton Company)	OTI	Entrance I	Same-floor – close to the door	38	120
		Entrance II	Same-floor – away from door		126
	ITI	LOS I	Open area with machinery	40	120
		LOS II	Straight walkway		126
Office (Atwater Kent Laboratories)	OTI	Entrance I & II	Same-floor – main& side	27	132
	ITI	NLOS	Rooms/corridors of 3rd floor	26	90
	RTI	AK3C	Corridors of 3rd floor	17	306
		offices	Small rooms		204
		labs	Large room		528
Total number of Measurements					3030

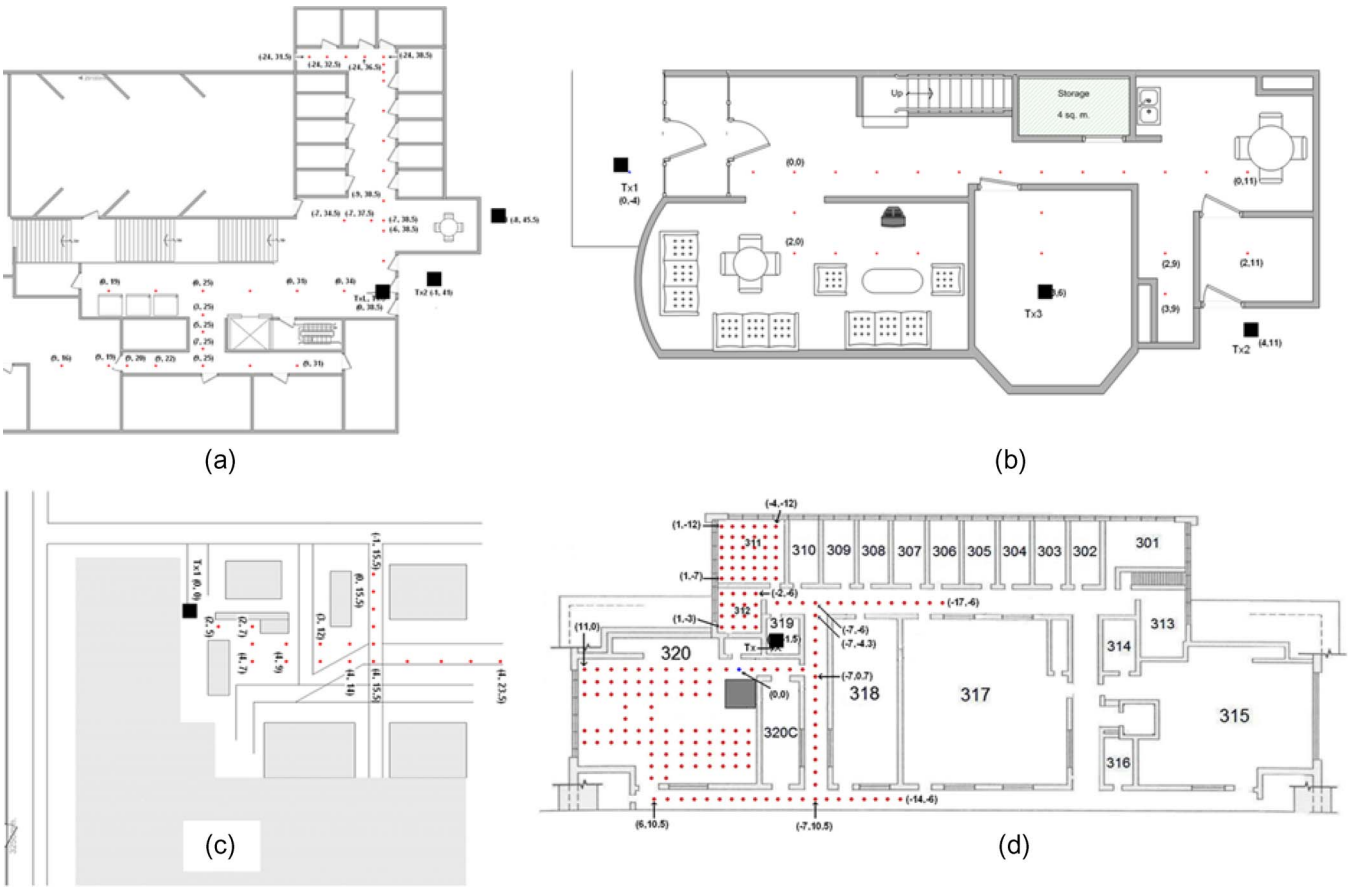

Fig. 2. Sample measurement floor plans. (a) Fuller OTI/ITI. (b) Schussler OTI/ITI. (c) Norton ITI. (d) AK RTI. (Squares: Tx locations. Dots: Rx locations).

dimensions on the order of a few hundred meters, and the floor is cluttered with machinery, equipment, and metallic beams. The AK building is a three-floor building that has a traditional office structure consisting of rooms that have dimensions on the order of a few meters. This building in particular has been used for measurements from the roof due to ease of accessibility.

In the campaign, three ranging scenarios were measured: ITI, OTI, and RTI. Table I describes the details of the measurement locations. ITI and OTI measurements were conducted in all the buildings. RTI measurements however were only conducted in the AK building. Fig. 2 shows sample floor plans with the measurement locations. In each measurement, the location of the transmitter was fixed, whereas the receiver was moved along certain grid points. Care was taken to expose the measurements to a variety of indoor NLOS conditions ranging from harsh obstacles, such as elevator shafts, metallic doors, and concrete walls, to other lighter wall structures, as this would provide a wide range of performance conditions.

Measuring $\hat{\alpha}_{\mathrm{DP}}$, and $\hat{\tau}_{\mathrm{DP}}$ or $\hat{\tau}_{\mathrm{NDP}}$ requires accurate *a priori* knowledge of the transmitter–receiver distances. This proved to be challenging since there was no direct LOS in the various locations that we measured. To tackle this problem and minimize the error incurred from physically measuring the distance, we devised a practical method to grid the building floor with transmitter and receiver locations. We created a 3-D Cartesian coordinate system with 1 m as its unit. We then placed grid points on the floor in the positions that we were interested in measuring and assigned x, y, and z coordinates to each point. For example, if the coordinates of the transmitter and the receiver are given by (x_A, y_A, z_A) and (x_B, y_B, z_B), respectively, then the distance can easily be found using the Euclidian relation, i.e.,

$$d_{AB} = \sqrt{(x_A - x_B)^2 + (y_A - y_B)^2 + (z_A - z_B)^2}. \qquad (9)$$

D. Postprocessing

In the postprocessing of channel measurement data, the time-domain channel impulse response is obtained by first passing the frequency-domain measurements through a Hanning window to reduce the noise sidelobes. Even though some other window functions such as the Kaiser window provides higher dynamic range, the Hanning window is selected for its much faster decaying sidelobes, which significantly reduces the interfering effect of strong MPCs in peak detection. The windowed frequency response is then converted to time domain through the inverse Fourier transform. For the analysis in this paper, 500-MHz and 3-GHz bandwidths were parsed out of the measured frequency-domain data with a center frequency of 4.5 GHz. The channel transfer function was divided into these frequency bands to reflect different potential UWB systems, i.e., multiband orthogonal division multiplexing and single-pulse transmission. In addition, the impact of bandwidth on the path loss exponent of the DP component and the ranging accuracy can be evaluated. Specifically, 500 MHz of bandwidth provides time-domain resolution on the order of $\Delta t_{500\,\mathrm{MHz}} = 2$ ns ≈ 0.6 m, whereas 3 GHz provides $\Delta t_{3\,\mathrm{GHz}} = 0.3$ ns ≈ 0.1 m. $\hat{\alpha}_{\mathrm{DP}}$ and $\hat{\tau}_{\mathrm{DP}}$ are then detected from the time-domain channel profile using a peak detection algorithm. The threshold for peak detection is set to -120 dB, which is the system's noise threshold. Identifying the presence or absence of the DP required analyzing the power in the bin of the expected TOA of the DP, which is related to the time-domain resolution Δt for that bandwidth. If a peak is detected within the bin, the DP is declared present. Otherwise, the DP is declared absent.

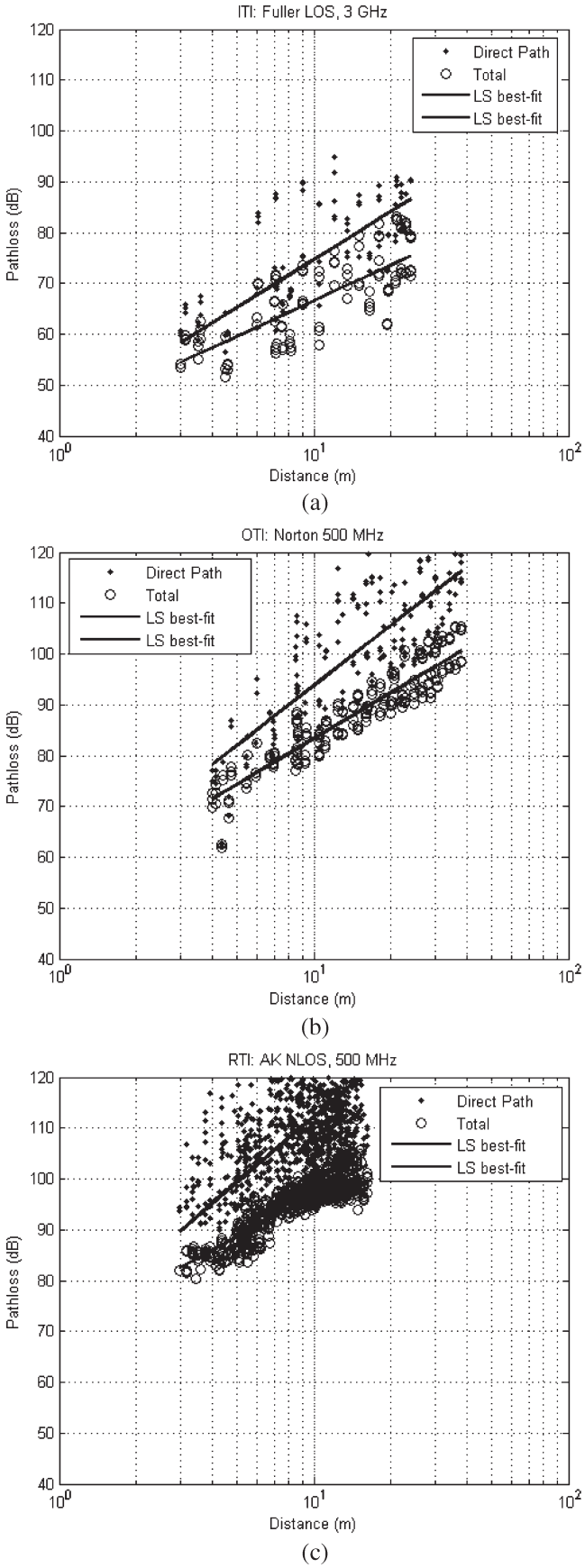

Fig. 3. Path loss scatter plots. (a) ITI Fuller (3 GHz). (b) OTI Norton (500 MHz). (c) RTI AK (500 MHz).

TABLE II
PATH LOSS PARAMETERS

Scenario	Environment	PL_p(dB)	Direct Path				Total Signal	
			500 MHz		3 GHz			
			γ	χ(dB)	γ	χ(dB)	γ	χ(dB)
ITI	Fuller (LOS)	0	3.2	8.9	3.3	7.1	2.4	5.5
	Norton (LOS/NLOS)	0	3.5	8.5	4.5	9.1	2.6	3.4
	Schussler (NLOS)	6	3.4	7.9	4.0	8.4	3.0	4.6
	AK (NLOS)	7.5	5.4	6.2	5.6	8.5	3.6	6.2
OTI	Fuller	14.3	3.4	13.7	3.7	14.1	2.2	7.7
	Norton	8.7	3.9	7.8	5.0	10.1	3.3	4.4
	Schussler	7.6	4.1	10.5	4.2	11.1	3.2	6.1
	AK	10	4.6	8.7	5.1	8.9	3.1	3.2
RTI	AK	24.5	4.3	7.6	5.3	8.8	2.9	1.7

IV. RANGING COVERAGE ANALYSIS

A. Modeling the Path Loss

Using the same established path-loss-modeling approach used in literature [17], [28], [31], we attempt to characterize the distance-power dependence of the measured DP, which, we believe, is important in assessing the ranging coverage and the performance of UWB indoor geolocation systems [15]. The distance-power gradient is determined from the measurement data through least-square (LS) linear regression [28]. The path loss expression in decibels at some distance d is given by

$$PL(d) = PL_0 + 10\gamma \log_{10}\left(\frac{d}{d_0}\right) + \chi, \qquad d \geq d_0 \quad (10)$$

where PL_0 is the path loss at $d_0 = 1$ m; $10\gamma \log_{10}(d/d_0)$ is the average path loss with reference to d_0; γ is the path loss exponent, which is a function of the measured scenario, building environment, and bandwidth; and χ is the lognormal shadow fading.

B. Result

We present our results by grouping different ranging scenarios and environments. For both ITI and OTI, we provide results for the Norton, Fuller, Schussler, and AK buildings. For RTI, we provide results for the AK building only.

Fig. 3 shows sample measured scatter plots of the path loss as a function of the TX–RX separation for different buildings and ranging scenarios. The straight line is the best-fit LS linear regression. Like many other models in literature, the value of PL_0 is found through fitting the data to (10). We observed that the intercept value changed according to the ranging scenarios and building environments. Therefore, we measured PL_0 at 1 m in free space to be around 42 dB and added another parameter to compensate for the penetration loss. Therefore, the modification to the model in (10) is given by

$$PL(d) = PL_0 + PL_p + 10\gamma \log_{10}\left(\frac{d}{d_0}\right) + \chi, \qquad d \geq d_0 \quad (11)$$

where PL_p is the penetration loss and varies according to the measurement condition. Table II provides a summary of the path loss results. Several observations can be made from the table and the figures. The first is that, for all the measurement data, the path loss exponent is higher for the DP compared to the total signal power, which justifies our modeling approach. Second, the DP power experiences greater fluctuations around the mean path loss, compared to the total signal counterpart. This observation makes sense, because small variations on the transmitter location affect the DP power more than the total power. Third, PL_p changes for the different penetration scenarios. In ITI scenarios, Schussler NLOS suffers a 6-dB penetration loss due to the walls, compared to the 7.5-dB penetration loss in AK. Norton ITI measurements are a mixture of LOS/NLOS, because the manufacturing floor contained scattered machinery. The impact can clearly be seen on the path loss exponent when the bandwidth increases, hence yielding higher attenuation. The results of the OTI measurements show that Fuller and AK exhibit the largest penetration loss, mainly because the signal had to penetrate a heavier construction when compared to Norton and Schussler. In addition, the path loss exponents in AK are large, mainly because the measurement locations were conducted inside a metal shop on the edge of the building and between concrete corridors and rooms. AK, in general, imposes a very challenging environment for ranging because of the building material and dense cluttering. The RTI measurements experienced the largest penetration loss and a high path loss exponent. Finally, note that the harsher the indoor environment, the higher the path loss exponent difference when moving to a higher system bandwidth. This is mainly due to the fact that larger system bandwidths provide better time-domain resolutions at the cost of reduced power per MPC. This implies that the advantage of higher time-domain resolution comes at a cost of shorter ranging coverage.

V. RANGING ERROR ANALYSIS

A. Spatial Characterization

The goal of our modeling efforts is to provide tools to simulate the spatial ranging error behavior in indoor environments for two popular UWB system bandwidths. Ranging errors have been modeled using different approaches. In [13] and [33], they were modeled as a combination of Gaussian and exponential distributions using ray-tracing simulation software and through measurements, respectively. The latter refined the technique of the former and added an additional classification of extreme NLOS. The main problem with this approach is that it is not based on any system model; therefore, it lacks physical

significance. Alternatively, our modeling approach will focus on the behavior of errors in the presence and absence of the DP similar to [21].

The spatial characteristics of the ranging errors are determined by the behavior of the biases, which are random due to the unknown structure of the indoor environment and the relative location of the user to them. Since the errors are highly dependent on the absence or presence of the DP, we will model it according to the error classification in Section II. Furthermore, to model and compare the behavior in different building environments and scenarios, the normalized ranging error will be modeled instead. This is given by

$$\psi = \frac{\varepsilon}{d} = \frac{(\hat{d} - d)}{d}. \tag{12}$$

The range error experienced in an indoor environment can then be modeled by combining the conditions in (6) and (7) through the following expression:

$$\psi = \psi_m + G(\psi_{\mathrm{pd}} + X\psi_B) \tag{13}$$

where ψ_m is the normalized multipath error that exists in both the presence and absence of the DP. ψ_{pd} is the normalized propagation-delay-induced error. ψ_B is the normalized error due to DP blockage. To distinguish between the error behavior in LOS and NLOS, we use a Bernoulli random variable G. That is

$$G = \begin{cases} 0, & \text{LOS} \\ 1, & \text{NLOS} \end{cases} \tag{14}$$

where $p(G = 0) = p(\text{LOS})$ is the probability of being in LOS, and $p(G = 1) = p(\text{NLOS})$ is the probability of being in NLOS. Similarly, X is a Bernoulli random variable that models the occurrence of DP blockage given by

$$X = \begin{cases} 0, & \zeta_1 \\ 1, & \zeta_2 \end{cases} \tag{15}$$

where $p(X = 1) = p(\zeta_2)$ denotes the probability of the occurrence of blockage, and $p(X = 0) = p(\zeta_1)$ denotes the probability of detecting a DP. Again, we clarify that our modeling approach specifically focuses on the DP and not on the traditional definition of NLOS used for communications. This means that an MT and an RP separated by a wall, for instance, is considered NLOS but does not necessarily mean the absence of the DP. In the remainder of this paper, ranging error, bias, and normalized error will interchangeably be used, and they will refer to (13).

B. Probability of DP Blockage

The probability of an MT within the ranging coverage of an RP to experience DP blockage depends on the system SNR, bandwidth, building environment, ranging scenario, and the relative location and density of scattering objects. Table III reports the measured blockage probabilities $p(\zeta_2)$. Several observations can be concluded. First, a positive correlation between the system bandwidth and the blockage probability $p(\zeta_2)$ exists due to lower energy per MPCs in the higher system bandwidth. Second, as expected, DP blockage increases from ITI to OTI and RTI. Attenuation due to penetration from exterior walls and ceiling results in higher $p(\zeta_2)$. Third, blockage is highly correlated with the building type. In residential environments, blockage probability is low since the interior is composed of wooden structures with a few metallic objects (e.g., a fridge and laundry room). Office buildings, however, pose harsher conditions with thicker walls, metallic beams, vending machines, metallic cabinets, shelves, and elevator shafts, resulting in a substantial blockage of up to 90% (see Fuller and AK ITI/OTI). In addition, ITI measurements in the manufacturing floor highlight the impact of the occasional clutter of machinery. Finally, it is worth mentioning that these results were measured using a 120-dB dynamic range provided by the external amplifiers and LNA extending the measured range. In realistic UWB systems, unfortunately, this is truly not the case, which means that the results here can be seen as a lower bound.

TABLE III
PROBABILITY OF DP BLOCKAGE

Scenario	Environment	500 MHz		3 GHz	
		$\%\zeta_1$	$\%\zeta_2$	$\%\zeta_1$	$\%\zeta_1$
ITI	Fuller	10	90	2	98
	Norton	96	4	83	17
	Schussler	89	11	87	13
	AK	39	61	32	68
OTI	Fuller	42	58	39	61
	Norton	57	43	24	76
	Schussler	77	23	60	40
	AK	40	60	22	78
RTI	AK	58	42	37	63

C. Error Behavior in the Presence of the DP

Ranging in the presence of the DP occurs in LOS and NLOS environments. In the former, the experienced errors are small and mainly due to the multipath. In the latter, however, the impact of multipath is further emphasized through scattering (diffractions) and DP attenuation. Furthermore, propagation delays, albeit a nuisance parameter in some instances, can, in some situations, cause further degradation on the ranging estimate. The measurement results of the ranging error in LOS scenarios revealed that the impact of the multipath can be modeled through a normal distribution. This can explicitly be given by

$$f(\psi|G = 0) = \frac{1}{\sqrt{2\pi\sigma_m^2}} \exp\left[-\frac{(\psi - \mu_m)^2}{2\sigma_m^2}\right] \tag{16}$$

with mean μ_m and standard deviation σ_m that are specific to the LOS multipath induced errors. Fig. 4 further confirms the normality of errors in this condition. A similar observation of the multipath effect in indoor LOS environments has been reported through measurements [21]. In NLOS scenarios, when the DP is present, the amount of propagation delay and multipath due to obstructing objects such as wooden walls causes the biases to be more positive. The results show (see Fig. 5) that the spatial characteristics retain the statistics of the LOS counterpart but with a higher mean and standard deviation. According to these

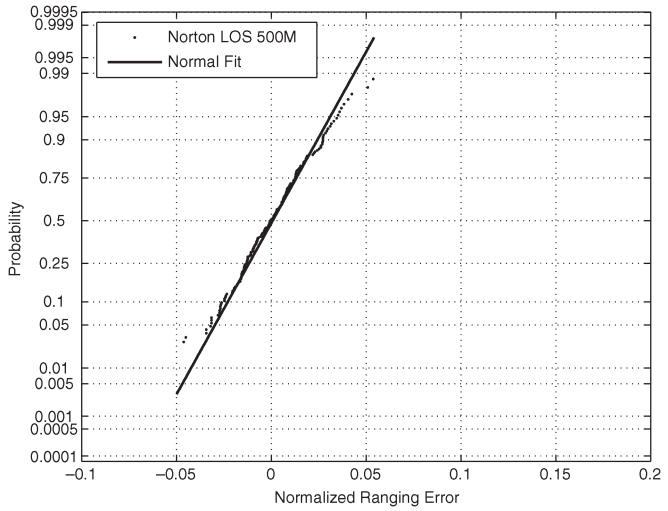

Fig. 4. ITI Norton-500 MHz. Confirming the normality of the biases.

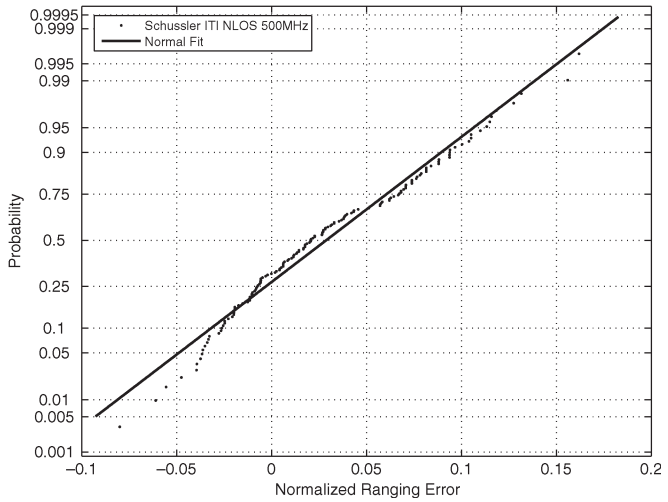

Fig. 5. Schussler ITI NLOS. The mean of the biases is larger than LOS.

results, we model the normalized ranging error similar to (16) but with emphasis on the condition. This is given by

$$f\left(\psi|G=1,X=0\right)=\frac{1}{\sqrt{2\pi\sigma_{m,\mathrm{pd}}^{2}}}\exp\left[-\frac{(\psi-\mu_{m,\mathrm{pd}})^{2}}{2\sigma_{m,\mathrm{pd}}^{2}}\right]. \tag{17}$$

The subscripts in (17) specify the contributing error factors. Table IV provides the modeling parameters of all the scenarios and environments in the presence of the DP. The results show a positive correlation between the statistics of the normal distribution with the complexity of environment and/or ranging scenarios. A negative correlation can be seen between the statistics and the system bandwidth due to the reduction of multipath error in higher bandwidths.

D. Error Behavior in the Absence of the DP

The shadowing of the DP impacts the error behavior in several ways. First, only positive errors occur since the blockage induces a higher positive bias that dominates compared with the multipath counterpart. Second, there are occasionally large positive range errors that occur due to heavier indoor constructions, such as elevator shafts, clustering of cabinets, or even metallic doors. Third, the diversity of blocking material in indoor environments means that the spatial distribution of errors will, in general, exhibit a heavier positive tail. By examining the probability density functions (PDFs) of the measured ranging errors in this condition, we observed that different subsets of the data showed varying tail behaviors. The "heaviness" of the tail depended on the ranging environment and scenario. Thus, harsher blockage conditions, i.e., higher number of blocked MPCs, exhibited heavier tails. This critical observation led us to consider distributions with different tail characteristics.

TABLE IV
DP NORMAL DISTRIBUTION MODELING PARAMETERS

Scenario	Environment	500 MHz		3 GHz	
		μ_m	σ_m	μ_m	σ_m
ITI	Fuller (LOS)	0	0.028	0	0.006
	Norton (LOS)	0	0.022	0	0.007
		$\mu_{m,pd}$	$\sigma_{m,pd}$	$\mu_{m,pd}$	$\sigma_{m,pd}$
	Fuller (NLOS)	0.058	0.028	0.003	0.01
	Schussler (NLOS)	0.029	0.047	0.014	0.016
	AK (NLOS)	0.023	0.020	0.009	0.004
OTI	Fuller	0.015	0.017	0.002	0.011
	Norton	0.019	0.029	0.002	0.015
	Schussler	0.041	0.045	0.011	0.013
	AK	0.034	0.023	0.012	0.004
RTI	AK	0.029	0.041	0.012	0.012

To accurately model the measurement data, we select distributions that are known to have the ability to fit data with different tail behaviors. Among them are exponential, lognormal, Weibull, and generalized extreme value (GEV). The class of GEV distributions is very flexible with a specific tail parameter that controls the shape and size of the tail, in addition to the location and scale parameters. It has been applied to model extreme events in hydrology, climatology, finance, and insurance industries [34], [35].

To determine the goodness-of-fit of these different distributions to the data, we apply the Kolmogorov–Smirnov (K-S) hypothesis test at 5% significance level. In addition, we fit the data to the normal distribution to verify its lack of suitability in characterizing the spatial distribution of the ranging error in this condition. This is specifically important since normality is usually assumed as a model for the ranging error in localization performance analysis. Table V compares the passing rates of the K-S test for the aforementioned distributions. The results show that both the normal and exponential distributions are not valid models for the ranging error in the absence of the DP, because they are consistently poor in passing the K-S test, i.e., below 80% for most data sets. Similarly, for the Weibull distribution, most of the passing rate is below 90%. Comparing these results with the GEV and lognormal distributions, it is possible to see that their passing rate is above 90% for most of the data sets. Only in ITI Schussler is their performances similar to those in Weibull and normal distributions, which is mainly due to the lightness of the tail. In addition, GEV distribution

TABLE V
PASSING RATE OF THE K-S HYPOTHESIS TEST AT 5% SIGNIFICANCE LEVEL

Scenario	Normal		Exponential		GEV		Lognormal		Weibull	
	0.5 GHz	3 GHz	0.5 GHz	3 GHz	0.5 GHz	3 GHz	0.5 GHz	3 GHz	0.5 GHz	3 GHz
ITI Fuller	70.8	68.8	85.1	83.3	91.7	86.4	90.7	88.1	85.1	85.3
ITI Norton	76.3	75.9	70.7	62.7	88.1	86.3	87.3	82.4	83.2	79.8
ITI Schussler	83.2	72.3	67.8	66.5	85.7	82.8	84.7	78.7	85.1	74.8
ITI AK	84.4	75.5	67.7	74.6	91.6	84.7	91.7	76.2	92.8	76.9
OTI Fuller	80.8	79.2	85.2	88.5	92.9	90.8	94.0	92.7	89.8	91.4
OTI Norton	80.2	83.1	75.9	71.4	92.1	93.9	91.6	90.5	86.5	88.1
OTI Schussler	77.3	86.9	68.7	71.2	91.9	94.5	89.0	93.4	82.7	89.7
OTI AK	80.1	78.1	69.1	76.2	89.1	84.5	88.3	89.4	83.1	85.5
RTI AK	85.4	87.6	72.3	76.3	96.9	94.0	93.9	95.4	89.8	91.6

passing rates are close to the lognormal. For some data sets, the difference between their passing rates is less than 2%. As a result, these two distributions are the best candidates for modeling the tail behavior of errors in the absence of the DP. The GEV distribution models the tail behavior with three degrees of freedom, compared to two in the lognormal distribution, providing enhanced flexibility in capturing the error statistics in a variety of circumstances. It is defined as

$$f(x;\xi,\mu,\sigma)=\frac{1}{\sigma}\exp\left(-\left(1+\xi\left(\frac{x-\mu}{\sigma}\right)\right)^{-1/\xi}\right)\times\left(1+\xi\left(\frac{x-\mu}{\sigma}\right)\right)^{-1-\frac{1}{\xi}} \tag{18}$$

for $1+\xi(x-\mu)/\sigma>0$, where μ, σ, and ξ are the location, scale, and shape parameters, respectively. GEV combines three simpler distributions in the form given in (18). The value of the shape parameter specifies the type of distribution. Type I (Gumbel) corresponds to $\xi=0$. Type II (Frechet) corresponds to $\xi>0$. Type III (Weibull) corresponds to $\xi<0$. The Gumbel and Weibull in the GEV sense correspond to the mirror images of the usual distributions [36]. The normalized error data in all the measurement sets in the absence of the DP fit the Frechet type of the GEV. Although this is a possible fit to our data, we chose lognormal instead for the following reasons: First, the K-S test performance of the lognormal distribution is close to the GEV, which attests to the ability of the former in modeling the data with two degrees of freedom compared with three in the latter. Second, the simplicity of the lognormal model compared with the GEV makes its application in localization bounds analysis, e.g., generalized CRLB, analytically more feasible (see [26]).

The lognormal model is then given by

$$f(\psi|G=1,X=1)=\frac{1}{\psi\sqrt{2\pi\sigma^2_{m,\mathrm{pd},B}}}\exp\left[-\frac{(\ln\psi-\mu_{m,\mathrm{pd},B})^2}{2\sigma^2_{m,\mathrm{pd},B}}\right] \tag{19}$$

where $\mu_{m,\mathrm{pd},B}$ and $\sigma_{m,\mathrm{pd},B}$ are the mean and standard deviation of the ranging error's logarithm, respectively. The subscripts emphasize the contributing factors. Fig. 6 provides sample measurement results confirming the lognormal behavior of the error. The estimated parameters of the lognormal distribution, which is obtained using maximum-likelihood estimation techniques, for different ranging scenarios and environments are given in Table VI.

Similar observations compared to earlier models can be observed for the correlation between the error statistics with bandwidth and ranging conditions. However, there are several scenarios where the extent of the correlation diminishes. For example, Fuller OTI and ITI contain measurements in dense cluttered environments, and increase in the system bandwidth has limited impact on the parameters of the model. This is mainly due to the ranging conditions that induce large blockage errors that are effectively insensitive to bandwidth changes, e.g., elevator shafts.

VI. SIMULATION RESULT

A. Predicting Ranging Coverage

To predict the ranging coverage for different environments and scenarios, we simulated the average DP path loss using (11) according to the model parameters in Table II and calculated R_c according to the definition in (4) for different values of system dynamic range ρ. Fig. 7 provides the results of ranging coverage simulations against different system dynamic ranges for 500-MHz and 3-GHz system bandwidths. As reflected in the measurement results, RTI faces the toughest constraint for ranging. The simulation reveals that, for a dynamic range of around 100 dB and a bandwidth of 500 MHz, the ranging coverage for AK RTI and OTI is less than 10 m. For other OTI environments, it is about 15 m, whereas ITI varies between 25 and 60 m, depending on the LOS or NLOS conditions. Another observation from the simulation results is that the change in system bandwidth substantially reduces the coverage. This is less the case for *pure* LOS scenarios, where the coverage is almost the same for both bandwidths (see ITI Fuller). The other ITI environments, however, are mixed LOS/NLOS for Norton and *pure* NLOS for Schussler and AK. This is clearly reflected in the change of their coverage between the bandwidths.

B. Simulating Ranging Error

The models presented in Section V provide a very simple yet realistic and flexible approach to statistically characterizing ranging errors experienced in typical indoor environments. Model parameters G and X provide control over the LOS/NLOS and the presence/absence of the DP conditions, respectively. The model distribution parameters then provide control over the error experienced in each condition. To further validate our modeling approach, we simulate the normalized

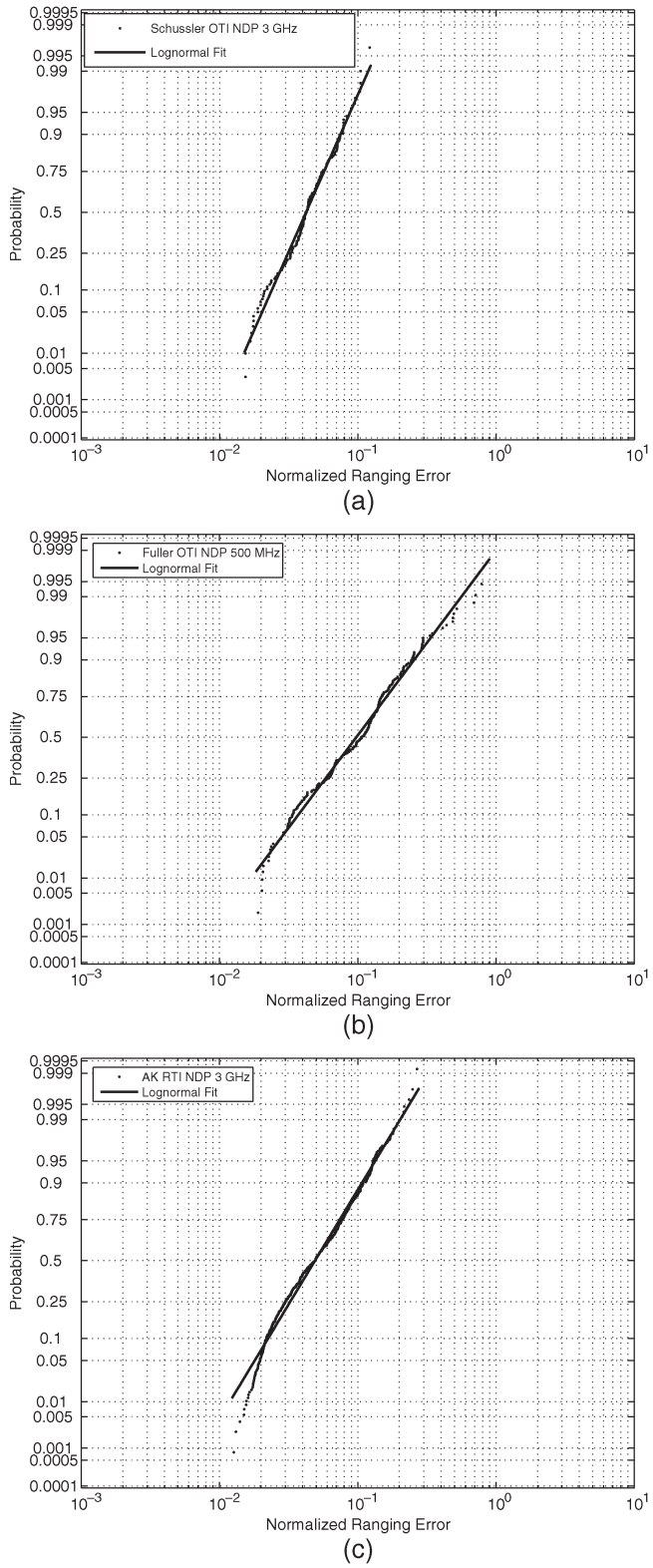

Fig. 6. Confirming the lognormal fit of the measured normalized ranging error. (a) Schussler OTI 3 GHz. (b) Fuller OTI 500 MHz. (c) AK RTI 3 GHz.

TABLE VI
LOGNORMAL DISTRIBUTION MODELING PARAMETERS

Scenari	Environment	500 MHz		3 GHz	
		$\mu_{m,pd,B}$	$\sigma_{m,pd,B}$	$\mu_{m,pd,B}$	$\sigma_{m,pd,B}$
ITI	Norton (NLOS)	-3.13	0.62	-4.29	0.45
	Fuller (NLOS)	-1.68	0.88	-1.90	1.13
	Schussler (NLOS)	-1.59	0.49	-2.72	0.53
	AK (NLOS)	-2.17	0.45	-2.89	0.81
OTI	Fuller	-2.33	0.75	-2.99	1.17
	Norton	-2.78	0.65	-3.82	0.52
	Schussler	-2.03	0.58	-3.16	0.45
	AK	-2.32	0.51	-3.11	0.77
RTI	AK	-1.99	0.54	-3.01	0.61

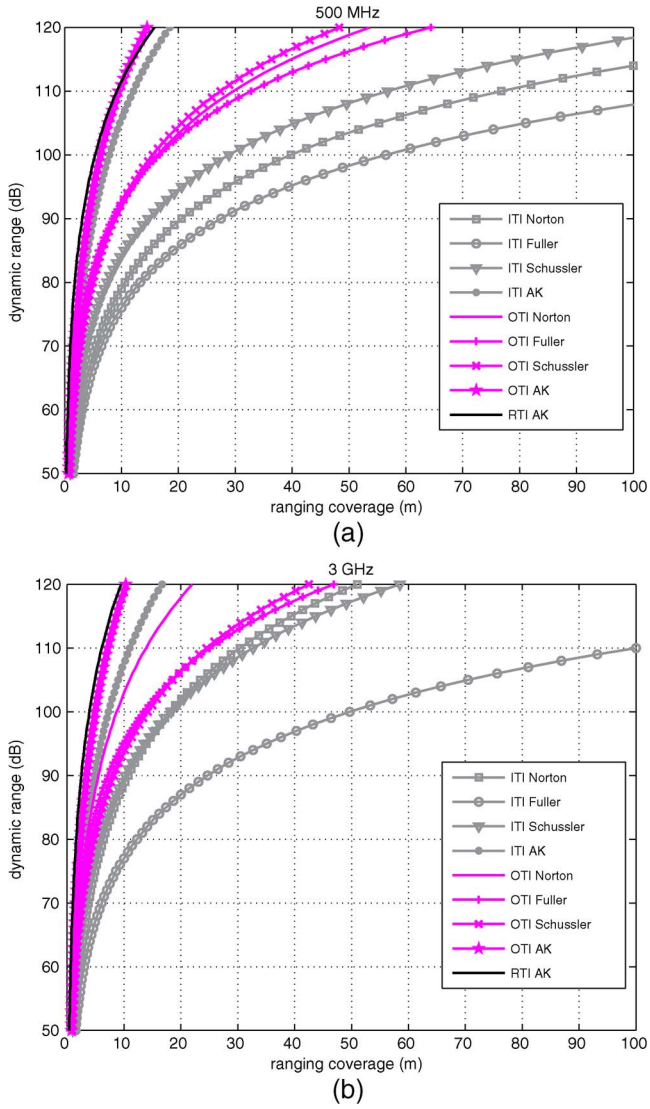

Fig. 7. Simulated ranging coverage.(a) 500-MHz bandwidth. (b) 3-GHz bandwidth.

ranging error according to the models in Section V and compare them to the measurements. For each ranging condition and scenario, we run Monte Carlo simulations with 10 000 normalized range error samples. We focus on NLOS conditions since performance in LOS is intuitive and has sufficiently been addressed in the literature. Therefore, we set $p(G = 1) = 1$, and for each sample, we ran a Bernoulli trial with $p(X = 1) = p(\zeta_2)$, from Table III, where the outcome determines the distribution, i.e., whether (17) or (19). The simulated samples are stacked in a vector, and their cumulative distribution

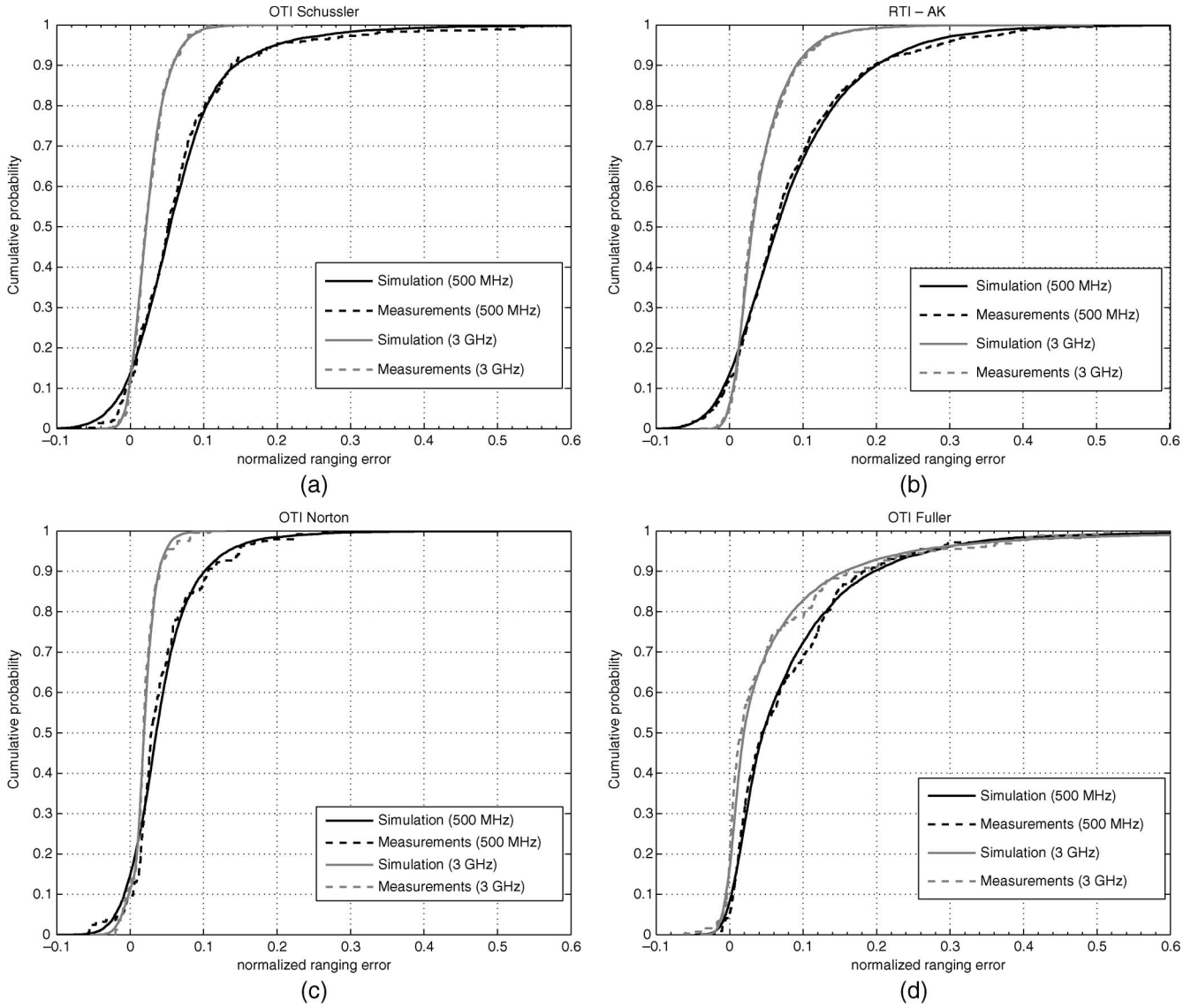

Fig. 8. CDF of the simulated normalized ranging error versus the measurements. (a) OTI Schussler. (b) RTI AK. (c) OTI Norton. (d) OTI Fuller.

function (CDF) is compared with the measurement data set in that specific scenario and environment. Fig. 8 provides several examples comparing the results of simulation to the measurements. The models show close agreement to the measurements. This is mainly because the model has the ability to statistically describe the error in ζ_1 and ζ_2 independently. This approach provides flexibility in modeling the factors contributing to the error, which will be different, depending on the ranging situation. For instance, if several MTs are scattered in an indoor environment and the RPs are fixed in different locations in and surrounding the building, then the ranging error PDF of all the range estimates can be described according to these models. The error distribution will vary from heavy tailed to normally distributed, as the range conditions change from extreme NLOS to LOS.

VII. Conclusion

In this paper, we have described a comprehensive UWB measurement and modeling campaign that characterized the spatial ranging error and coverage of TOA-based ranging in indoor environments. The measurements involved four different building environments, i.e., a house, an old office, a modern office, and a manufacturing floor, and three different ranging scenarios, i.e., ITI, OTI, and RTI. We showed that the ranging coverage is inversely related to the bandwidth of the system and the harshness of the ranging scenario and environment. In addition, the statistics of the measured ranging error showed that they follow normal and lognormal distributions in the presence and absence of the DP, respectively. Furthermore, the distribution parameters are affected by the ranging scenario, environment, and system bandwidth.

The measurement and modeling results in this paper provide an experimental analysis of the physical constraints imposed by the dense cluttered indoor environments on TOA-based UWB ranging. The results should aid researchers in deriving and analyzing wireless localization bounds that are specific to indoor environments. These localization bounds are necessary to understand the fundamental limitations facing UWB TOA-based localization systems and algorithms in these environments.

Future research in this area could focus on measuring and analyzing the ranging error beyond the ranging coverage. Specifically, the behavior of the biases and measurement time variations with distance must be evaluated for different ranging scenarios and environments. Finally, research in localization algorithms for indoor-specific wireless networks is needed to identify and mitigate NLOS biased range measurements to achieve acceptable localization performance.

REFERENCES

[1] D. Porcino and W. Hirt, "Ultra-wideband radio technology: Potential and challenges ahead," *IEEE Commun. Mag.*, vol. 41, no. 7, pp. 66–74, Jul. 2003.

[2] M. Ghavami, L. B. Michael, and R. Kohno, *Ultra-Wideband Signals and Systems in Communication Engineering*. Hoboken, NJ: Wiley, 2004.

[3] I. Oppermann, M. Hamalainen, and J. Iinatti, *UWB Theory and Applications*. Hoboken, NJ: Wiley, 2004.

[4] S. Gezici, Z. Tian, G. B. Giannakis, H. Kobayashi, A. F. Molisch, H. V. Poor, and Z. Sahinoglu, "Localization via ultra-wideband radios: A look at positioning aspects for future sensor networks," *IEEE Signal Process. Mag.*, vol. 22, no. 4, pp. 70–84, Jul. 2005.

[5] K. Pahlavan, X. Li, and J. Makela, "Indoor geolocation science and technology," *IEEE Commun. Mag.*, vol. 40, no. 2, pp. 112–118, Feb. 2002.

[6] R. J. Fontana and J. Gunderson, "Ultra-wideband precision asset location system," in *Proc. IEEE Conf. UWBST*, May 2002, pp. 47–150.

[7] J. Y. Lee and R. A. Scholtz, "Ranging in a dense multipath environment using an UWB radio link," *IEEE J. Sel. Areas Commun.*, vol. 20, no. 9, pp. 1677–1683, Dec. 2002.

[8] K. Pahlavan, P. Krishnamurthy, and J. Beneat, "Wideband radio propagation modeling for indoor geolocation applications," *IEEE Commun. Mag.*, vol. 36, no. 4, pp. 60–65, Apr. 1998.

[9] W. C. Chung and D. Ha, "An accurate ultra wideband (UWB) ranging for precision asset location," in *Proc. IEEE Conf. UWBST*, Reston, VA, Nov. 2003, pp. 389–393.

[10] B. Alavi and K. Pahlavan, "Bandwidth effect on distance error modeling for indoor geolocation," in *Proc. IEEE Conf. Pers., Indoor Mobile Radio Commun.*, Beijing, China, Sep. 2003, vol. 3, pp. 2198–2202.

[11] Z. Tarique, W. Q. Malik, and D. J. Edwards, "Bandwidth requirements for accurate detection of direct path in multipath environment," *Electron. Lett.*, vol. 42, no. 2, pp. 100–102, Jan. 2006.

[12] K. Pahlavan, F. O. Akgul, M. Heidari, A. Hatami, J. M. Elwell, and R. D. Tingley, "Indoor geolocation in the absence of the direct path," *IEEE Wireless Commun. Mag.*, vol. 13, no. 6, pp. 50–58, Dec. 2006.

[13] B. Denis and N. Daniele, "NLOS ranging error mitigation in a distributed positioning algorithm for indoor UWB ad-hoc networks," in *Proc. IEEE IWWAN*, Oulu, Finland, May/Jun. 2004, pp. 356–360.

[14] J.-Y. Lee and S. Yoo, "Large error performance of UWB ranging in multipath and multiuser environments," *IEEE Trans. Microw. Theory Tech.*, vol. 54, no. 4, pp. 1887–1895, Jun. 2006.

[15] N. Alsindi, B. Alavi, and K. Pahlavan, "Empirical pathloss model for indoor geolocation using UWB measurements," *Electron. Lett.*, vol. 43, no. 7, pp. 370–372, Mar. 2007.

[16] A. F. Molisch, "Ultrawideband propagation channel-theory, measurement and modeling," *IEEE Trans. Veh. Technol.*, vol. 54, no. 5, pp. 1528–1545, Sep. 2005.

[17] S. S. Ghassemzadeh, R. Jana, C. W. Rice, W. Turin, and V. Tarokh, "Measurement and modeling of an ultra-wide bandwidth indoor channel," *IEEE Trans. Commun.*, vol. 52, no. 10, pp. 1786–1796, Oct. 2004.

[18] A. Muqaibel, A. Safaai-Jazi, A. Attiya, B. Woerner, and S. Riad, "Pathloss and time dispersion parameters for indoor UWB propagation," *IEEE Trans. Wireless Commun.*, vol. 5, no. 3, pp. 550–559, Mar. 2006.

[19] C.-C. Chong and S. K. Yong, "A generic statistical-based UWB channel model for high-rise apartments," *IEEE Trans. Antennas Propag.*, vol. 53, no. 8, pp. 2389–2399, Aug. 2005.

[20] C. Falsi, D. Dardari, L. Mucchi, and M. Z. Win, "Time of arrival estimation for UWB localizers in realistic environments," *EURASIP J. Appl. Signal Process.*, vol. 2006, no. 17, pp. 32 082-1–32 082-13, 2006.

[21] B. Alavi and K. Pahlavan, "Modeling of the TOA-based distance measurement error using UWB indoor radio measurements," *IEEE Commun. Lett.*, vol. 10, no. 4, pp. 275–277, Apr. 2006.

[22] N. Patwari, A. O. Hero, M. Perkins, N. S. Correal, and R. J. O'Dea, "Relative location estimation in wireless sensor networks," *IEEE Trans. Signal Process.*, vol. 51, no. 8, pp. 2137–2148, Aug. 2003.

[23] A. Hatami, K. Pahlavan, M. Heidari, and F. Akgul, "On RSS and TOA based indoor geolocation—A comparative performance evaluation," in *Proc. IEEE WCNC*, Las Vegas, NV, Apr. 2006, vol. 4, pp. 2267–2272.

[24] B. Alavi and K. Pahlavan, "Analysis of undetected direct path in time of arrival based UWB indoor geolocation," in *Proc. IEEE Veh. Technol. Conf.*, Dallas, TX, Sep. 2005, vol. 4, pp. 2627–2631.

[25] Z. N. Low, J. H. Cheong, C. L. Law, W. T. Ng, and Y. J. Lee, "Pulse detection algorithm for line-of-sight (LOS) UWB ranging applications," *IEEE Antennas Wireless Propag. Lett.*, vol. 4, pp. 63–67, 2005.

[26] Y. Qi, H. Kobayashi, and H. Suda, "Analysis of wireless geolocation in a non-line-of-sight environment," *IEEE Trans. Wireless Commun.*, vol. 5, no. 3, pp. 672–681, Mar. 2006.

[27] D. B. Jourdan, D. Dardari, and M. Z. Win, "Position error bound for UWB localization in dense cluttered environments," in *Proc. IEEE ICC*, Istanbul, Turkey, Jun. 2006, vol. 8, pp. 3705–3710.

[28] K. Pahlavan and A. H. Levesque, *Wireless Information Networks*, 2nd ed. Hoboken, NJ: Wiley, 2005.

[29] P. Krishnamurthy and K. Pahlavan, "Analysis of the probability of detecting the DLOS path for geolocation applications in indoor areas," in *Proc. IEEE 49th Veh. Technol. Conf.*, Houston, TX, Jul. 1999, vol. 2, pp. 1161–1165.

[30] K. Siwiak, H. Bertoni, and S. M. Yano, "Relation between multipath and wave propagation attenuation," *Electron. Lett.*, vol. 39, no. 1, pp. 142–143, Jan. 2003.

[31] S. J. Howard and K. Pahlavan, "Measurement and analysis of the indoor radio channel in the frequency domain," *IEEE Trans. Instrum. Meas.*, vol. 39, no. 5, pp. 751–755, Oct. 1990.

[32] B. Alavi, N. Alsindi, and K. Pahlavan, "UWB channel measurements for accurate indoor localization," in *Proc. IEEE MILCOM*, Washington DC, Sep. 2006, pp. 1–7.

[33] B. Alavi and K. Pahlavan, "Modeling of the distance error for indoor geolocation," in *Proc. IEEE WCNC*, New Orleans, LA, Mar. 2003, vol. 1, pp. 668–672.

[34] S. Markose and A. Alentorn, "Option pricing and the implied tail index with the generalized extreme value distribution," *Comput. Econom. Finance*, Nov. 2005. no. 397, Society for Computation Economics.

[35] J. Berlant, Y. Goegebeur, J. Segers, and J. Teugels, *Statistics of Extremes: Theory and Applications*. Hoboken, NJ: Wiley, 2004.

[36] E. Castillo, *Extreme Value Theory in Engineering*. New York: Academic, 1988.

Nayef A. Alsindi (S'02) received the B.S.E.E degree from the University of Michigan, Ann Arbor, in 2000 and the M.S. degree in electrical engineering from Worcester Polytechnic Institute (WPI), Worcester, MA, in 2004, where is currently working toward the Ph.D. degree in electrical and computer engineering with the Center for Wireless information Network Studies, Department of Electrical and Computer Engineering.

From 2000 to 2002, he was a Technical Engineer with Bahrain Telecommunications. From 2002 to 2004, he received a Fulbright Scholarship to pursue the M.S. degree at WPI. His research interests include the performance limitations of time-of-arrival-based ultrawideband ranging in indoor nonline-of-sight (NLOS) conditions, cooperative localization for indoor wireless sensor networks, and NLOS/blockage identification and mitigation.

Bardia Alavi (S'97–M'05) received the B.S. degree in electronics and the M.S. degree in telecommunication systems from Sharif University of Technology, Tehran, Iran, in 1997 and 1999, respectively, and the Ph.D. degree in electrical engineering from the Center for Wireless Information Network Studies, Worcester Polytechnic Institute, Worcester, MA, in 2006.

He is currently with the Wireless Networking Business Unit, Cisco Systems Inc., Richfield, OH. His research interests include indoor positioning and wireless channel characterization.

Kaveh Pahlavan (M'76–SM'81–F'87) received the M.S. degree in electrical engineering from the University of Tehran, Teheran, Iran, in 1975 and the Ph.D. degree in electrical engineering from the Worcester Polytechnic Institute, Worcester, MA, in 1979.

He is currently a Professor of electrical and computer engineering, a Professor of computer science, and the Director of the Center for Wireless Information Network Studies, Worcester Polytechnic Institute, Worcester, MA. He is also a Visiting Professor with the Telecommunication Laboratory and the Center for Wireless Communications, University of Oulu, Oulu, Finland. He is a coauthor of *Wireless Information Networks* (Wiley, 1995, 2005) with A. Levesque and *Principles of Wireless Networks—A Unified Approach* (Prentice–Hall, 2002) with P. Krishnamurthy.

Prof. Pahlavan is the Editor-in-Chief of the *International Journal of Wireless Information Networks*; a Member of the advisory board of the *IEEE Wireless Magazine*; a Member of the Executive Committee of the IEEE International Symposium on Personal, Indoor, and Mobile Radio Communications; was a Nokia Fellow in 1999; and was a Fulbright-Nokia Scholar in 2000. He has served as the general chair and organizer of a number of successful IEEE events and has contributed to numerous seminal technical and visionary publications in wireless office information networks, home networking, and indoor geolocation science and technology.